ACS NANO

www.acsnano.org

ARTICLE

Room-Temperature Polariton Lasing from CdSe Core-Only Nanoplatelets

Francisco Freire-Fernández,[‖] Nathan G. Sinai,[‖] Max Jin Hui Tan, Sang-Min Park, Eric Rodolfo Koessler, Todd Krauss,* Pengfei Huo,* and Teri W. Odom*

Cite This: *ACS Nano* 2024, 18, 15177−15184

Read Online

ACCESS | Metrics & More | Article Recommendations | Supporting Information

ABSTRACT: **This paper reports how CdSe core-only nanoplatelets (NPLs) coupled with plasmonic Al nanoparticle lattices can exhibit exciton-polariton lasing. By improving a procedure to synthesize monodisperse 4-monolayer CdSe NPLs, we could resolve polariton decay dynamics and pathways. Experiment and theory confirmed that the system is in the strong coupling regime based on anticrossings in the dispersion diagrams and magnitude of the Rabi-splitting values. Notably, polariton lasing is observed only for cavity lattice periodicities that exhibit specific dispersive characteristics that enable polariton accumulation. The threshold of polariton lasing is 25-fold lower than the reported photon lasing values from CdSe NPLs in similar cavity designs. This open-cavity platform offers a simple approach to control exciton polaritons anticipated to benefit quantum information processing, optoelectronics, and chemical reactions.**

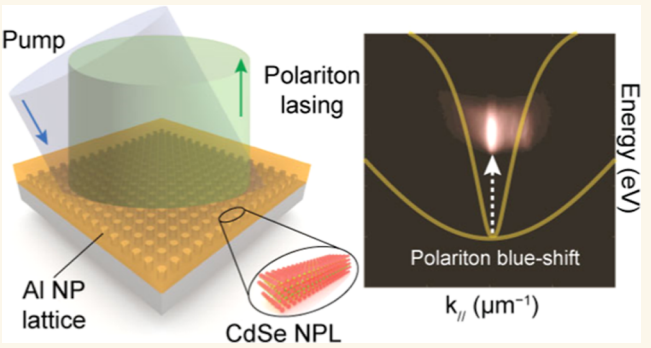

KEYWORDS: *polariton lasing, strong coupling, CdSe nanoplatelets, nanoparticle arrays, surface lattice resonances*

Strong light-matter coupling and the generation of exciton-polaritons are attracting attention in quantum information processing,[1,2] optical and spin-based electronic devices,[3,4] and controlling chemical reactivity.[5,6] Polaritons are hybrid light-matter states that form when the interaction strength between an optical cavity and emitter exceeds the individual losses. In a strongly coupled system, energy is coherently exchanged between the electronic state of the emitter and the optical mode of the cavity.[7,8] Recently, polaritons have been pursued to understand mechanisms of light generation since, unlike photon lasing, polariton lasing does not depend on the population inversion of excited states but on the buildup of polariton population in the same quantum state.[9,10] Since the coherent emission of photons by radiative decay of polaritons occurs spontaneously, polariton lasing occurs at considerably lower thresholds.[9,11] This distinct property has resulted in prospects to realize electrically driven, room temperature polariton lasing by optimizing both gain material and cavity design.[12−15]

Semiconducting CdSe nanoplatelets (NPLs) are promising exciton materials for strong coupling because of their out-of-plane quantum confinement in 1D and large in-plane oscillator strength.[16,17] Compared to other emitters used in strongly coupled systems (e.g., organic dyes,[18] emissive metal−organic frameworks,[19] and perovskites[15,20,21]), the crystal structure of CdSe NPLs results in increased chemical stability;[22] moreover, their exciton states can be n- or p-doped under an applied voltage.[23] CdSe NPL excitons can be delocalized across their entire 2D area, which minimizes nonradiative optical losses from biexciton Auger recombination;[24,25] the presence of defects can, however, result in exciton localization.[26] These features have enabled amplified spontaneous emission as well as photon lasing under pulsed[27,28] and continuous-wave pump excitation.[29]

The primary approach to reducing thresholds using CdSe NPLs as gain material has focused on core/shell engineering or lateral size modulation to mitigate Auger-based losses.[24,25] However, polariton lasing offers an alternative route to realizing efficient coherent light sources. Previous studies have demonstrated strong coupling using core-only CdSe NPLs in Fabry−Pérot,[30] gold film,[31] and nanohole array[32] cavities but polariton lasing has not been reported. Plasmonic

Received: March 6, 2024
Revised: May 6, 2024
Accepted: May 15, 2024
Published: May 29, 2024

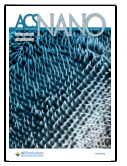

https://doi.org/10.1021/acsnano.4c03164
ACS Nano 2024, 18, 15177−15184

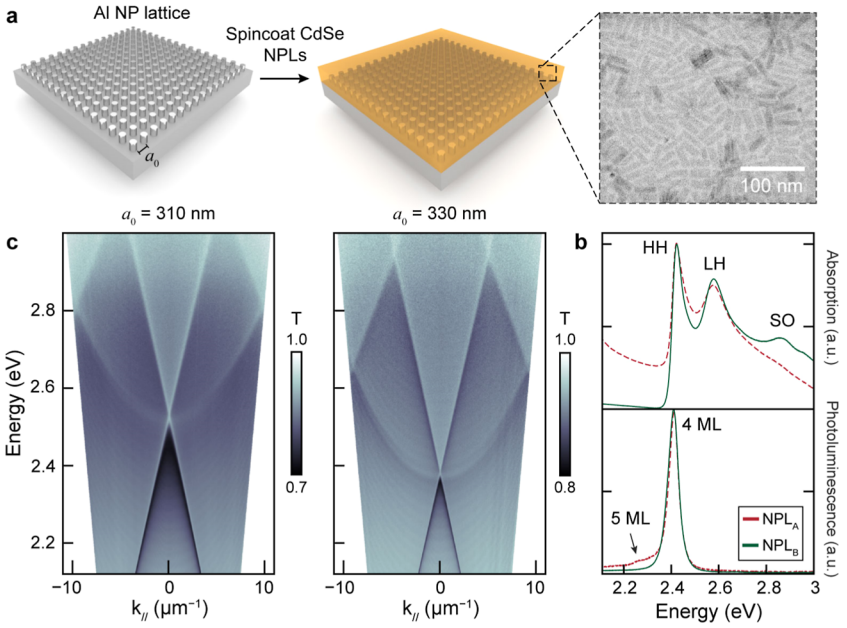

Figure 1. Strongly coupled CdSe NPL-Al nanoparticle lattice system. (a) Scheme of components. Inset shows a TEM image of CdSe NPL$_B$. (b) Absorption and photoluminescence spectra of NPL$_A$ and NPL$_B$ batches. (c) TE-polarized optical transmission dispersion diagrams of bare Al nanoparticle lattices with different periodicities, a_0.

nanoparticle lattices are attractive cavities for polariton lasing given that they are a well-established cavity for photon lasing; their large scattering cross sections from the localized surface plasmons of nanoparticles combined with the in-plane diffraction (Rayleigh anomaly (RA)) modes[33−35] form surface lattice resonances (SLRs) that support distributed feedback.[36−41] In addition, SLR modes exhibit polarization-dependent dispersion properties.[33,35] Importantly, strong coupling using these cavities with organic dyes,[18,42] metal−organic frameworks,[19] and 2D perovskites,[20] has been reported where the open-cavity architecture of plasmonic lattices enabled precise tuning over the degree of coupling.

Here, we show room-temperature polariton lasing from CdSe NPL films strongly coupled to plasmonic Al nanoparticle lattices. By optimizing the synthesis and purification protocol to produce monodisperse 4-monolayer CdSe NPLs, we could differentiate polariton decay dynamics from that of common CdSe impurities. We discovered that although strong coupling was supported by different lattice periodicities, polariton lasing was observed only at specific exciton-cavity detuning. Angle-resolved transmission measurements exhibited anticrossing and band-bending signatures that closely matched Jaynes−Cummings−Hopfield calculations; the fitted Rabi splitting energies were in the strong coupling regime. When the devices were optically pumped, lasing from the lower polariton (LP) band was observed at a threshold of ∼6 μJ/cm^2, 25 times lower than values reported for photon lasing. The polaritonic nature of the emission was supported by static and time-resolved photoluminescence measurements below the lasing threshold and Holstein−Tavis−Cummings calculations.

RESULTS AND DISCUSSION

Figure 1a depicts the light and matter components for a strongly coupled system based on an Al plasmonic nanoparticle lattice coated with a CdSe NPL thin film. Al nanoparticles (height $h \approx 55$ nm, diameter $d \approx 95$ nm) were patterned by electron-beam lithography on high-refractive index (n) glass substrates ($n_{glass} \approx 1.578$ @ 500 nm) to reduce refractive index differences with the CdSe NPL films ($n_{film} \approx 1.73$ @ 475 nm, thickness $t = 95$ nm) that can result in hybrid optical modes,[43] including waveguide-SLRs[32,38,44] (Figure S1) with more complicated features. Synthesis of 4-monolayer (ML) CdSe NPLs generally followed reported protocols,[27,45,46] but we modified and scaled the procedure to achieve monodisperse 4 ML CdSe NPLs with high brightness (Supporting Information: S1). Transmission electron microscopy of NPLs from our optimized protocol shows uniform lateral sizes of about 10 nm × 30 nm (Figure 1a). Although the synthesis of CdSe NPLs has been widely adopted,[27,29,45,47,48] we discovered that the quality of products depended critically on the initial degassing of the reagents. We speculate that this step involves the formation of CdSe seeds, which can then direct NPL growth. For comparison, we synthesized and purified two CdSe NPL batches under the same conditions except for the degassing step: (1) at 80 °C for 1 h according to literature[27] (NPL$_A$); and (2) at 95 °C for 30 min in our modified procedure (NPL$_B$). Films were produced by concentrating NPL solutions to 60 mg/mL in cyclohexane and then spin-casting at 4000 rpm on transparent substrates (Supporting Information: S2).

Figure 1b shows both the normalized absorption and photoluminescence of CdSe NPL$_A$ and NPL$_B$ films. In both batches, the absorption spectra had two distinct bands (2.42 and 2.58 eV) that can be assigned as heavy hole (HH) and light hole (LH) excitons, respectively. However, the spin−orbit split-off band (SO) at 2.86 eV was exclusively detected in NPL$_B$, and CdSe NPL$_A$ exhibited a broad absorption feature below the HH band; these differences could be from the inhomogeneous lateral dimensions of the NPL$_A$ batch (Figure S2). When the films were excited at low fluences (ca. 0.8 μJ/cm^2) and at 420 nm (1 kHz, 100 fs), the photoluminescence showed a single emission band for CdSe NPL$_B$ films but also a weak 5 ML emission peak for CdSe NPL$_A$ films. Although the percentage of 5 ML in CdSe NPL$_A$ is small, fluorescence resonance energy transfer within a 4 and 5 ML mixture can

https://doi.org/10.1021/acsnano.4c03164
ACS Nano 2024, 18, 15177−15184

convolute carrier lifetime measurements of strongly coupled systems.[49] Also, similar sample heterogeneities are known to result in energy funneling from large to small band gap semiconductors, which can result in higher thresholds for amplified spontaneous emission and lasing. Therefore, we use the improved CdSe NPL_B (referred to hereafter as NPL) materials for the strong coupling and polariton lasing study that follows.

To realize strong coupling with our optimized 4 ML CdSe NPLs, we designed Al nanoparticle lattices with varying periods (a_0) that support Γ-point ($k_{\|}$ = 0) SLR modes above (a_0 = 270 nm), between (a_0 = 310 nm), and below (a_0 = 330 nm) the LH and HH exciton energies. Figure 1c shows the angle-resolved transmission of Al lattices for a_0 = 310 and 330 nm; data for a_0 = 270 nm are in Figure S3. Transmission dispersion measurements for bare Al nanoparticle lattices under transverse-electric (TE)-polarized white light exhibit linear dispersive bands that follow the (±1,0) diffraction orders. Both bright and dark modes are observed about the Γ-point where the bands cross, which can be approximated by the Bragg diffraction equation $\lambda = a_0 \times n$. For lattices with a_0 = 310 nm, the band edge occurs at 2.52 eV, between the LH and HH energies, and for a_0 = 330 nm, it occurs at 2.38 eV, below the HH energy. We note an increase in SLR quality (i.e., narrower line widths) with increased lattice periodicity because of larger detuning of the RA condition from the localized surface plasmon of the nanoparticles, which were kept fixed in size and hence energy (2.70 eV) for all periodicities (Figure S5).[34,50] The transverse magnetic (TM)-polarized dispersion diagrams have quadratic bands and show trends of line width narrowing and band edge lowering similar to that under TE polarization (Figure S4).

Figure 2 compares experimental and calculated dispersion diagrams of a_0 = 310 and 330 nm Al nanoparticle lattices strongly coupled to CdSe NPL films under TE- and TM-polarized light. For both lattice periodicities, the transmission bands are markedly different from bare, uncoupled lattices in Figure 1c and exhibit the characteristic band anticrossing and band bending of polariton modes. Polariton bands with energies lower than the HH band are identified as lower polaritons (LP); the middle polaritons (MP) are between the HH and LH energies; and the upper polaritons (UP) reside above the LH energy. For the a_0 = 310 nm lattice (Figure 2a), the TE-polarized transmission shows two distinct LP band behaviors above and below the band gap (ca. 2.36 eV): (1) a nearly flat band that terminates at the dark edge of the band near the Γ-point and (2) linear bands that start at the bright edge. The MP and UP bands are relatively flat at large $k_{\|}$ values and become more dispersive as they approach $k_{\|}$ = 0. Similarly, three polariton bands are experimentally observed for a_0 = 330 nm lattices (Figure 2b). The LP bands shift to lower energies and become more intense, which makes the dark band edge more visible. These measurements indicate how a variety of distinct polariton dispersion characteristics can be achieved by tuning the Γ-point SLR energies with respect to the CdSe NPL exciton bands.

To confirm that our system is in the strong coupling regime, we used the Jaynes-Cummings model to extract Rabi splitting values (Ω) (Figures S6–S7).[18] The model estimates Ω values of 150 meV for the a_0 = 270 nm lattice and 130 meV for a_0 = 310 and 330 nm lattices. When compared with the exciton (γ_{HH}, γ_{LH}) and SLR (γ_{SLR}) loss factors (full-width half-maximum (fwhm) of the uncoupled exciton bands and SLR

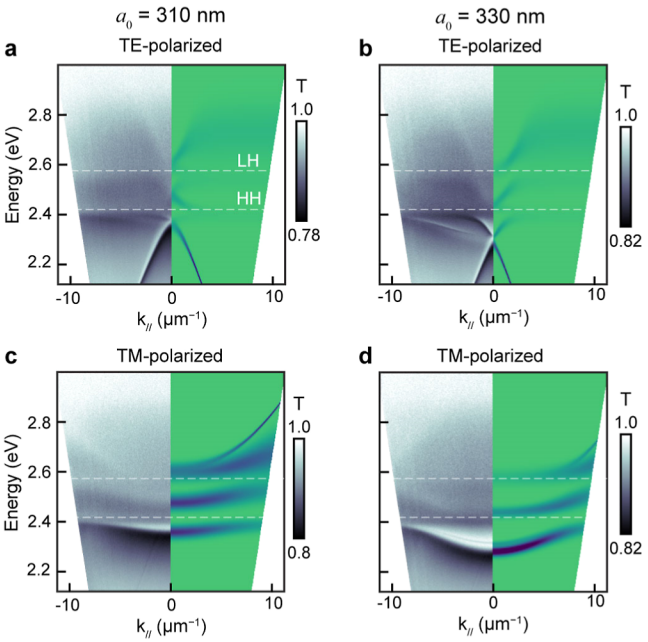

Figure 2. Polarization-dependent polariton dispersion diagrams. Experiment (left) and Jaynes–Cummings simulation (right) optical transmission of CdSe NPL films coupled to Al nanoparticle lattices under TE-polarized light with (a) a_0 = 310 nm and (b) a_0 = 330 nm and under TM-polarized light with (c) a_0 = 310 nm and (d) a_0 = 330 nm. The dashed lines indicate the energies of the light-hole (LH) and heavy-hole (HH) exciton bands.

band at the anticrossing position) (Tables S1–S2), the strong coupling conditions $\Omega > \gamma_{SLR}$ and $\Omega > \gamma_{HH,LH}$ are satisfied;[7] although the HH is strongly coupled to the a_0 = 270 nm lattice, the LH is not according to $\Omega < \gamma_{SLR}$ (Table S2). The right half of each plot in Figure 2 shows the simulated transmission diagrams with line widths and relative intensities of the polariton bands based on their Hopfield coefficients and uncoupled SLR eigenmode properties.[51,52] The modeling is in good agreement with the experiment; slight discrepancies may be attributed to approximations intrinsic to this model (Supporting Information: S6–S7).

Since SLR modes are polarization dependent, strong coupling resulted in polariton bands with distinct dispersion behavior under TM-polarized (versus TE-polarized) light (Figure 2c,d). TM-polariton bands have local minima at $k_{\|}$ = 0 and show increasingly dispersive character at larger $k_{\|}$ values. As the lattice periodicity a_0 of the cavity increased, the polariton bands became narrower while maintaining their flat-banded dispersion (Figures S3, 2a,b). One important feature of the strongly coupled a_0 = 330 nm lattice under TM illumination is the presence of two LP bands (Figure 2d): a slightly blue-shifted, LP band with a higher quality factor (Q) and a more intense LP band of lower Q. These LP bands formed from the RA and SLR cavity modes of the plasmonic lattice (Figure S4). That there are two LP bands with distinct Q in experiment and theory indicates that both RA and SLR modes can be simultaneously and independently strongly coupled to CdSe NPL excitons. To distinguish between polaritons from RA and SLR modes, we label them as LP_{RA} and LP_{SLR}, respectively.

To characterize the emission of the strongly coupled system, we performed angle-resolved photoluminescence experiments using a Fourier microscopy setup with a 1 kHz, 100 fs pulsed

https://doi.org/10.1021/acsnano.4c03164
ACS Nano 2024, 18, 15177–15184

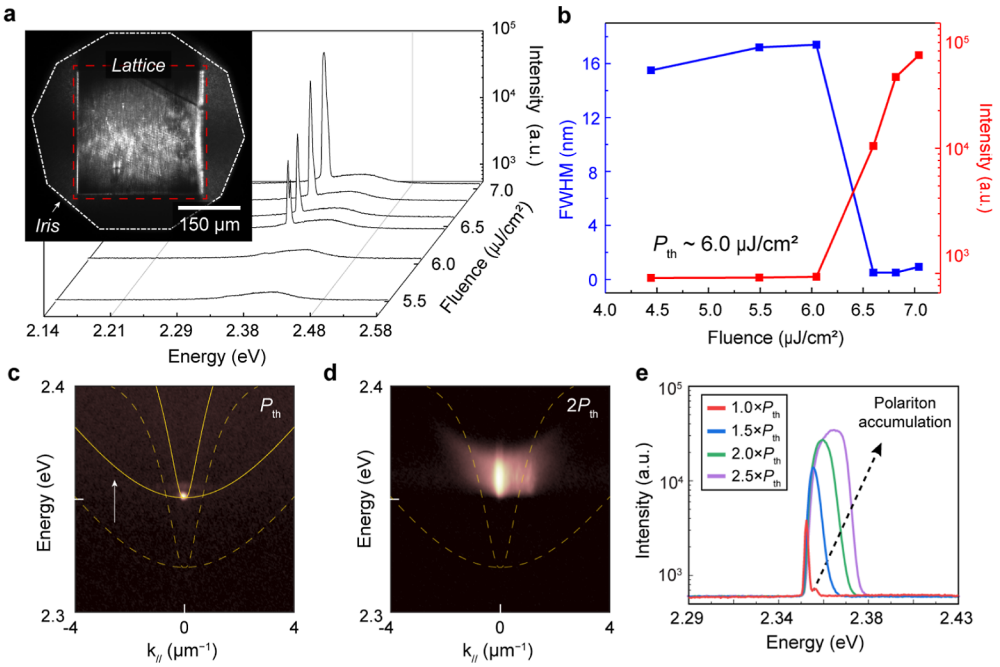

Figure 3. Polariton lasing from a_0 = 330 nm lattice. (a) Waterfall plot of emission intensity and wavelength as a function of pump fluence. Inset shows the real space image of the lattice above the lasing threshold P_{th}. (b) Input−output plot showing a linear to superlinear increase in intensity along with rapid line width narrowing at $P_{th} \approx 6\ \mu J/cm^2$. (c) Angle-resolved photoluminescence image at P_{th} shows that lasing is slightly blue-shifted at the lasing threshold. LP bands above (below) the threshold are indicated in solid (dashed) lines. The solid line is a guide to the eye where the calculated LP bands were shifted. (d) Angle-resolved photoluminescence image at 12 $\mu J/cm^2$ reveals band broadening and further blue shifting above the threshold of the LP bands. (e) Above-threshold spectral traces taken at the Γ-point confirm a gradual peak shift and broadening, as expected from polariton−polariton interactions.

excitation source centered at 420 nm. Surprisingly, lasing resulted only from the a_0 = 330 nm lattice that showed the largest negative detuning from the HH exciton, even though the other cavity periodicities also supported strong coupling. Figure 3a shows a nonlinear increase in the photoluminescence as a function of excitation fluence characteristic of lasing action. At low pump fluence (<5.5 $\mu J/cm^2$), only a broad photoluminescence feature from uncoupled NPL excitons was observed around 2.42 eV; however, upon increased fluence, an intense and narrow lasing peak at higher energies ca. 2.35 eV (fwhm = 1.8 meV, 0.4 nm) emerged. The inset in Figure 3 indicates that the lasing emission is delocalized across the entire pump areas, a common feature of plasmonic lattice cavity lasers.[53] Pump fluence vs output intensity curves show behavior expected of lasing action, with a transition from linear to superlinear behavior accompanied by a rapid narrowing in line width (Figure 3b). Notably, the threshold fluence P_{th} = 6.0 $\mu J/cm^2$ is very low; compared to photon lasing using core-only CdSe NPLs ($P_{th} \approx$ 150−200 $\mu J/cm^2$),[27,28] this threshold is around 25-fold less. Despite higher optical losses intrinsic to plasmonic cavities, this low threshold is similar to dielectric-cavity lasers that integrate gain-engineered materials such as core/crown CdSe NPLs or lead halide perovskite nanocrystals.[54−56]

To determine whether lasing was mediated by photons or polaritons, we used angle-resolved photoluminescence imaging to identify which bands contributed to the signal. At fluences near the threshold (Figure 3c), the LP emission occurs at the Γ-point and at an energy 25 meV higher than that of the isoenergetic TE-polarized dark band-edge SLR and TM-polarized LP_{RA} band (Figure 2b−d). The collapse of emission into the minima of the LP band suggests polariton−polariton relaxation and also that population accumulation at the minima is the mechanism behind the lasing observed, i.e., polariton lasing.[9] At twice the polariton lasing threshold, Figure 3d reveals that the emission broadens and shifts to higher energies. Normalized high-fluence spectral measurements (Figure 3e) confirm the gradual shift and broadening of the emission from 2.351 eV (fwhm = 1.8 meV, 0.4 nm) at P_{th} to 2.365 eV (fwhm = 14 meV, 3.5 nm) at 2.5 × P_{th}. Both the spectral blue-shifting and peak broadening can be attributed to polariton−polariton Coulombic repulsion and polariton-exciton repulsion since exciton−phonon coupling in CdSe NPLs is weak.[16,57] We note that the observed shift in lasing energy is distinct from multiexciton amplified spontaneous emission from uncoupled CdSe NPLs that show spectral red-shifts due to attractive multiexciton interactions.[27]

To understand why polariton lasing was observed only from the a_0 = 330 nm lattice, we characterized the photoluminescence of the strongly coupled system below the threshold (Figure 4). Since single-exciton emission in CdSe NPLs occurs as a band that is Stokes-shifted ∼7 meV from the HH absorption energy,[27,48] photoluminescence from polaritons will be limited primarily to LP bands and, in some cases, MP bands; emission from MP is fairly strong for a_0 = 270 nm (Figure S3). Although the transmission of the LP bands shows dark and bright SLR band edges negatively detuned from the HH band for both lattices (Figure 2), the photoluminescence shows additional differences. For the a_0 = 310 nm lattice, strong emission is observed from the LP bands, with higher intensities around the Γ-point region, as well as weaker emission from the MP (Figure 4a, inset). Since the LP band edges for the a_0 = 330 nm lattice are at lower energies than the HH, the regions of highest intensity are when $k_{||} > 5\ \mu m^{-1}$,

https://doi.org/10.1021/acsnano.4c03164
ACS Nano 2024, 18, 15177−15184

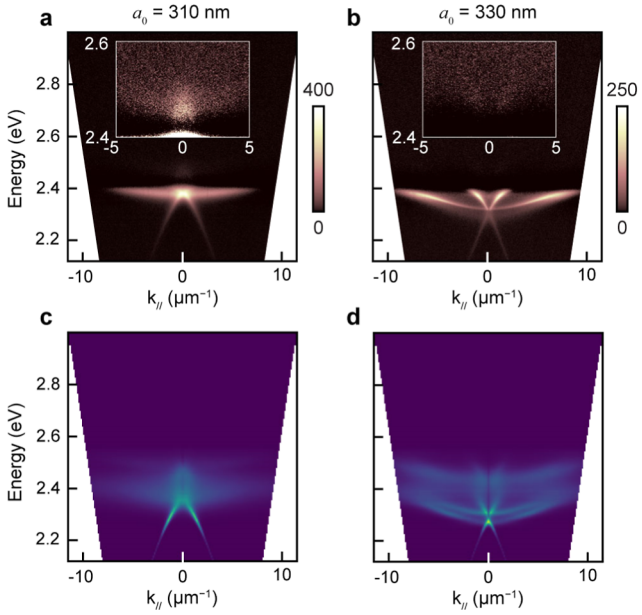

Figure 4. Cavity-dependent photoluminescence from the lower polariton. Experimental photoluminescence measurements of Al NP lattices coupled to CdSe NPL films with (a) a_0 = 310 nm and (b) a_0 = 330 nm. Insets in (a) and (b) are regions of middle polariton emission, displayed from 0 to 25 counts. These measurements are background subtracted from the uncoupled film. Simulated PL measurements from a generalized Holstein−Tavis−Cummings model with (c) a_0 = 310 nm and (d) a_0 = 330 nm.

particularly for TM-polarized LP bands (Figure 4b); only faint emission from MPs was measured (inset). Also, we calculated the photoluminescence using the generalized Holstein−Tavis−Cummings (GHTC) model[58] (Figure 4c,d), where the population dynamics were simulated using the Lindblad mean-field Ehrenfest method.[59] The photoluminescence spectra were generated by combining the polariton population dynamics and Hopfield coefficients of the GHTC exciton-polariton states. The intensities at each angle and energy were weighted by the polariton population and magnitude of SLR character in each state (Supporting Information: S8−S10). The model correctly predicted emission from the MP and LP bands, in agreement with experiments. Some minor discrepancies are found since the mean-field Ehrenfest dynamics method is known to overestimate the MP and UP populations when using a Holstein phonon-coupling model.[30]

The photoluminescence intensity distribution trends in Figure 4 indicate that cavities with different periodicities facilitate different polariton relaxation pathways. For the a_0 = 310 nm lattice, the buildup of the LP population occurs at the top of the bright, TE-polarized band edge; hence, polaritons populating this band edge can decay further along the LP band, which likely precludes polariton accumulation and therefore polariton lasing. In contrast, for the a_0 = 330 nm lattice, the TE-polarized LP bands are populated above the LP dark band edge at $k_{\|} > 5$ μm^{-1}, and polaritons can lower their energy through polariton−polariton scattering events to accumulate at the band minima. Moreover, although both lattices support TM-polarized LP bands with similar dispersive behavior, their line widths are different. For the a_0 = 310 nm lattice, polaritons populate the LP_{SLR} band; for the a_0 = 330 nm lattice, polaritons primarily populate the higher Q-factor LP_{RA} band and from which lasing is observed. Another determining factor for polariton lasing is the polariton radiative lifetime, which sets an upper limit for the rate that the polariton population can accumulate at the band minima and hence contribute to lasing. Fortunately, the high purity of our 4 ML CdSe NPLs allowed us to estimate uncoupled exciton and LP radiative lifetimes by performing time-resolved photoluminescence that integrated the entire (E, $k_{\|}$) response (Figure 4a,b) using a streak camera under nonresonant, pulsed excitation (420 nm, 0.8 μJ/cm^2) (Supporting Information: S11). We analyzed time-resolved traces of the LP emission energies below the single-exciton emission peak to extract the LP lifetimes.

Radiative decay of uncoupled CdSe NPL films follows a biexponential behavior with room-temperature time constants τ_1 and τ_2 on the order of 30−60 ps and 0.2−12 ns, respectively; the fast and slow decay components are attributed to the bright and dark exciton lifetimes.[16,17,45] For the uncoupled NPL film at 2.36 eV, our fitting produced τ_1 = 36.7 ps and τ_2 = 338.6 ps, in agreement with reported values.[16,17] The strongly coupled system also showed similar biexponential decays, where τ_1 can be assigned to a direct polariton radiative transition and τ_2 to transitions into the longer-lived dark polariton reservoir. Interestingly, the results for a_0 = 310 nm lattices (τ_1 = 32 ps and τ_2 = 313.3 ps) showed shorter radiative lifetimes than the uncoupled film, while the a_0 = 330 nm lattices (τ_1 = 37.6 ps and τ_2 = 319.8 ps) had longer lifetimes, which favors population accumulation (Supporting Information: S11). Photoluminescence and lifetime data suggest that for a_0 = 330 nm lattices, the LP bands facilitate efficient polariton relaxation and accumulation at the band minima, where a polariton population involved in lasing can build up because of their longer radiative lifetime. Similarly, polariton accumulation at the bright band edge of the a_0 = 310 nm lattice and the shorter polariton lifetime may have hindered polariton accumulation and therefore polariton lasing.

CONCLUSIONS

In summary, we demonstrated polariton lasing by tailoring dispersion diagrams of plasmonic lattices to support polariton relaxation and accumulation and improving the monodispersity of the CdSe NPL gain materials. Interestingly, this lattice cavity architecture can exhibit a rich range of polarization-dependent optical modes for strong coupling, including RA modes and SLRs. Our results highlight prospects for advances in polariton lasing by further engineering of particle shape and lattice geometry. Moreover, unlike the common Fabry−Pérot cavities, plasmonic lattices have an open architecture that allows ready interfacing with microfluidic devices as well as optical and electrochemical platforms to study polariton chemistry. We anticipate that ease in tuning polariton bands can be leveraged to modify the potential energy landscape of chemical reactions to increase the yield or achieve unexpected products, opening innovative tools for synthetic chemists.

METHODS

Sample Fabrication. Arrays of Al NPs were fabricated using electron-beam lithography (Raith Voyager) on PMMA A3 (Kayaku Advanced Materials)-coated H-BAK8 glass substrates (CDGM). After development, 55 nm of Al was electron-beam evaporated on the patterned substrates and then the photoresist was lifted off using acetone. Four monolayer CdSe core nanoplatelet films were spin-cast onto Al NP arrays by dropping 45 μL of a 60 mg/mL NPL solution while the substrate was spinning at 4000 rpm. The full synthesis and

https://doi.org/10.1021/acsnano.4c03164
ACS Nano 2024, 18, 15177−15184

purification protocols of the CdSe NPLs can be found in the Supporting Information.

Optical Characterization. Wavelength and angle-resolved transmission and PL measurements were carried out using a Fourier microscopy setup. The back focal plane of a 20× Plan Apo Nikon (NA = 0.75) objective lens was imaged onto the entrance slit of an SP2500 (Teledyne, Princeton Instruments) spectrometer coupled to a 2D CCD camera (PIXIS 400, Teledyne, Princeton Instruments). The images are then converted into $(E, k_{\|})$ plots where $E = hc/\lambda$ and $k_{\|} = (\omega/c)\sin\theta$, where h is the Planck constant, c is the speed of light in vacuum, λ is the wavelength, ω is the angular frequency, and θ is the incidence angle. During the transmission measurements, the samples were illuminated using a broadband white-light source, whose polarization was controlled to measure the optical response under TE or TM-polarized excitation.

During the PL and lasing experiments, the sample was excited at 420 nm by a laser system consisting of a tunable optical parameter amplifier (TOPAS Prime, Light Conversion) and a Solstice Ace (Spectra-Physics) mode-locked Ti:sapphire laser with a regenerative amplifier (fundamental 800 nm wavelength, 1000 Hz operation, and 100 fs pulse width). The laser excitation was incident at ca. 60° with respect to the sample normal and had a spot size of 3.45 mm by 1.7 mm. To remove the signal from uncoupled emitters in Figure 4, the PL was background subtracted against a pristine CdSe NPL film region located beside each array which minimized film heterogeneity effects. In the inset in Figure 3a, the pump beam spot size is larger than the imaged area and is filtered out during imaging using a long-pass filter.

Time-resolved photoluminescence measurements were performed using a streak camera (Hamamatsu) system with an Acton SP150 spectrometer (Princeton Instruments). During the experiments, the samples were excited at 420 nm with a fluence of 0.8 $\mu J/cm^2$ with the same laser system used in the lasing experiments. To image the full angular range captured by our Fourier microscopy setup, the back focal plane image of the collection objective lens was imaged onto the entrance slit of the spectrometer.

ASSOCIATED CONTENT

Supporting Information

The Supporting Information is available free of charge at https://pubs.acs.org/doi/10.1021/acsnano.4c03164.

CdSe NPL synthesis and purification; NPL and film characterization; additional optical characterization; localized surface plasmon mode simulation; details of fitting parameters; theoretical details of the SLR-mode dispersion; theoretical details of the $k_{\|}$-resolved transmission spectra simulations; theoretical details of the $k_{\|}$-resolved photoluminescence spectra simulations; details of the exciton−phonon coupling Hamiltonian; details of the quantum dynamics simulations; streak camera measurements and fittings (PDF)

AUTHOR INFORMATION

Corresponding Authors

Todd Krauss − *Department of Chemistry, University of Rochester, Rochester, New York 14627, United States; Institute of Optics, University of Rochester, Rochester, New York 14627, United States*; Email: todd.krauss@rochester.edu

Pengfei Huo − *Department of Chemistry, University of Rochester, Rochester, New York 14627, United States; Institute of Optics, University of Rochester, Rochester, New York 14627, United States*; orcid.org/0000-0002-8639-9299; Email: huo@chem.rochester.edu

Teri W. Odom − *Department of Chemistry, Northwestern University, Evanston, Illinois 60208, United States*; orcid.org/0000-0002-8490-292X; Email: todom@northwestern.edu

Authors

Francisco Freire-Fernández − *Department of Chemistry, Northwestern University, Evanston, Illinois 60208, United States*; orcid.org/0000-0002-6539-419X

Nathan G. Sinai − *Department of Chemistry, Northwestern University, Evanston, Illinois 60208, United States*; orcid.org/0000-0003-3507-992X

Max Jin Hui Tan − *Department of Chemistry, Northwestern University, Evanston, Illinois 60208, United States*

Sang-Min Park − *Department of Chemistry, Northwestern University, Evanston, Illinois 60208, United States*; orcid.org/0000-0002-4306-0375

Eric Rodolfo Koessler − *Department of Chemistry, University of Rochester, Rochester, New York 14627, United States*; orcid.org/0000-0001-9438-7530

Complete contact information is available at: https://pubs.acs.org/10.1021/acsnano.4c03164

Author Contributions

$^{\|}$F.F-F. and N.G.S. authors contributed equally.

Notes

The authors declare no competing financial interest.

ACKNOWLEDGMENTS

This work was supported by the National Science Foundation (NSF) Center for Quantum Electrodynamics for Selective Transformations (QuEST) (Grant CHE-2124398, N.G.S. E.K, S.M.P., P.H., T.D.K.), and the Vannevar Bush Faculty Fellowship from the U.S. Department of Defense (DOD N00014-17-1-3023, F.F.F., M.J.H.T., T.W.O.). This work made use of the NUFAB, EPIC, and SPID facilities of Northwestern University's NUANCE Center that has received support from the SHyNE Resource (NSF ECCS-2025633), the International Institute for Nanotechnology at Northwestern University (IIN), Northwestern's MRSEC Program (NSF DMR-1720139), and MRI (NSF DMR-1828676). M.J.H.T. and S.M.P. gratefully acknowledge support from the Ryan Fellowship and the IIN. This research was supported in part by the Quest high-performance computing facility at Northwestern University, which is jointly supported by the Office of the Provost, the Office for Research, and Northwestern University Information Technology. Computing resources were also provided by the Center for Integrated Research Computing (CIRC) at the University of Rochester. We also acknowledge Lele Mathis, Dr. Alexander D. Sample, and Dr. Xitlali G. Juarez at Northwestern University for initial assistance with sample fabrication and discussion and William Girten and Dr. Nicole M.B. Cogan at the University of Rochester for initial assistance with NPL synthesis and sample characterization.

REFERENCES

(1) Ghosh, S.; Liew, T. C. H. Quantum computing with exciton-polariton condensates. *npj Quantum Inf.* **2020**, *6*, 16.

(2) Kavokin, A.; Liew, T. C. H.; Schneider, C.; Lagoudakis, P. G.; Klembt, S.; Hoefling, S. Polariton condensates for classical and quantum computing. *Nat. Rev.* **2022**, *4*, 435−451.

(3) Dreismann, A.; Ohadi, H.; del Valle-Inclan Redondo, Y.; Balili, R.; Rubo, Y. G.; Tsintzos, S. I.; Deligeorgis, G.; Hatzopoulos, Z.; Savvidis, P. G.; Baumberg, J. J. A sub-femtojoule electrical spin-switch

based on optically trapped polariton condensates. *Nat. Mater.* **2016**, *15*, 1074−1078.
(4) Zasedatelev, A. V.; Baranikov, A. V.; Urbonas, D.; Scafirimuto, F.; Scherf, U.; Stöferle, T.; Mahrt, R. F.; Lagoudakis, P. G. A room-temperature organic polariton transistor. *Nat. Photonics* **2019**, *13*, 378−383.
(5) Tsintzos, S. I.; Pelekanos, N. T.; Konstantinidis, G.; Hatzopoulos, Z.; Savvidis, P. G. A GaAs polariton light-emitting diode operating near room temperature. *Nature* **2008**, *453*, 372−375.
(6) Wang, T.; Zang, Z.; Gao, Y.; Lyu, C.; Gu, P.; Yao, Y.; Peng, K.; Watanabe, K.; Taniguchi, T.; Liu, X.; et al. Electrically Pumped Polarized Exciton-Polaritons in a Halide Perovskite Microcavity. *Nano Lett.* **2022**, *22*, 5175−5181.
(7) Törmä, P.; Barnes, W. L. Strong coupling between surface plasmon polaritons and emitters: A review. *Rep. Prog. Phys.* **2015**, *78* (1), 013901.
(8) Hertzog, M.; Wang, M.; Mony, J.; Borjesson, K. Strong light-matter interactions: a new direction within chemistry. *Chem. Soc. Rev.* **2019**, *48* (3), 937−961. From NLM PubMed-not-MEDLINE
(9) Deng, H.; Weihs, G.; Snoke, D.; Bloch, J.; Yamamoto, Y. Polariton lasing vs. photon lasing in a semiconductor microcavity. *Proc. Natl. Acad. Sci. U.S.A.* **2003**, *100*, 15318−15323.
(10) Byrnes, T.; Kim, N. Y.; Yamamoto, Y. Exciton-polariton condensates. *Nat. Phys.* **2014**, *10* (11), 803−813.
(11) Bajoni, D. Erratum: Polariton lasers. Hybrid light-matter lasers without inversion. *J. Phys. D: Appl. Phys.* **2012**, *45* (31), 313001.
(12) Graf, A.; Held, M.; Zakharko, Y.; Tropf, L.; Gather, M. C.; Zaumseil, J. Electrical pumping and tuning of exciton-polaritons in carbon nanotube microcavities. *Nat. Mater.* **2017**, *16*, 911−917.
(13) Gu, J.; Chakraborty, B.; Khatoniar, M.; Menon, V. M. A room-temperature polariton light-emitting diode based on monolayer WS2. *Nat. Nanotechnol.* **2019**, *14*, 1024−1028.
(14) Schneider, C.; Rahimi-Iman, A.; Kim, N. Y.; Fischer, J.; Savenko, I. G.; Amthor, M.; Lermer, M.; Wolf, A.; Worschech, L.; Kulakovskii, V. D.; et al. An electrically pumped polariton laser. *Nature* **2013**, *497*, 348−352.
(15) Shang, Q.; Li, M.; Zhao, L.; Chen, D.; Zhang, S.; Chen, S.; Gao, P.; Shen, C.; Xing, J.; Xing, G.; et al. Role of the Exciton-Polariton in a Continuous-Wave Optically Pumped CsPbBr3Perovskite Laser. *Nano Lett.* **2020**, *20*, 6636−6643.
(16) Achtstein, A. W.; Schliwa, A.; Prudnikau, A.; Hardzei, M.; Artemyev, M. V.; Thomsen, C.; Woggon, U. Electronic structure and exciton-phonon interaction in two-dimensional colloidal cdse nanosheets. *Nano Lett.* **2012**, *12*, 3151−3157.
(17) Biadala, L.; Liu, F.; Tessier, M. D.; Yakovlev, D. R.; Dubertret, B.; Bayer, M. Recombination dynamics of band edge excitons in quasi-two-dimensional cdse nanoplatelets. *Nano Lett.* **2014**, *14*, 1134−1139.
(18) Ramezani, M.; Halpin, A.; Fernández-Domínguez, A. I.; Feist, J.; Rodriguez, S. R.-K.; Garcia-Vidal, F. J.; Gómez Rivas, J. Plasmon-exciton-polariton lasing. *Optica* **2017**, *4*, 31.
(19) Sample, A. D.; Guan, J.; Hu, J.; Reese, T.; Cherqui, C. R.; Park, J. E.; Freire-Fernández, F.; Schaller, R. D.; Schatz, G. C.; Odom, T. W. Strong Coupling between Plasmons and Molecular Excitons in Metal-Organic Frameworks. *Nano Lett.* **2021**, *21*, 7775−7780.
(20) Park, J. E.; López-Arteaga, R.; Sample, A. D.; Cherqui, C. R.; Spanopoulos, I.; Guan, J.; Kanatzidis, M. G.; Schatz, G. C.; Weiss, E. A.; Odom, T. W. Polariton Dynamics in Two-Dimensional Ruddlesden-Popper Perovskites Strongly Coupled with Plasmonic Lattices. *ACS Nano* **2022**, *16*, 3917−3925.
(21) Su, R.; Diederichs, C.; Wang, J.; Liew, T. C. H.; Zhao, J.; Liu, S.; Xu, W.; Chen, Z.; Xiong, Q. Room-Temperature Polariton Lasing in All-Inorganic Perovskite Nanoplatelets. *Nano Lett.* **2017**, *17*, 3982−3988.
(22) Ithurria, S.; Talapin, D. V. Colloidal Atomic Layer Deposition (c-ALD) using self-limiting reactions at nanocrystal surface coupled to phase transfer between polar and nonpolar media. *J. Am. Chem. Soc.* **2012**, *134*, 18585−18590.
(23) Huang, B.; Huang, Y.; Zhang, H.; Lu, X.; Gao, X.; Zhuang, S. Electrochemical Control over the Optical Properties of II-VI Colloidal Nanoplatelets by Tailoring the Station of Extra Charge Carriers. *ACS Appl. Mater. Interfaces* **2023**, *15*, 21354−21363.
(24) Kunneman, L. T.; Tessier, M. D.; Heuclin, H.; Dubertret, B.; Aulin, Y. V.; Grozema, F. C.; Schins, J. M.; Siebbeles, L. D. A. Bimolecular auger recombination of electron-hole pairs in two-dimensional CdSe and CdSe/CdZnS core/shell nanoplatelets. *J. Phys. Chem. Lett.* **2013**, *4*, 3574−3578.
(25) Yu, J.; Chen, R. Optical properties and applications of two-dimensional CdSe nanoplatelets. *InfoMat* **2020**, *2*, 905−927.
(26) Geiregat, P.; Rodá, C.; Tanghe, I.; Singh, S.; Di Giacomo, A.; Lebrun, D.; Grimaldi, G.; Maes, J.; Van Thourhout, D.; Moreels, I.; et al. Localization-limited exciton oscillator strength in colloidal CdSe nanoplatelets revealed by the optically induced stark effect. *Light: Sci. Appl.* **2021**, *10*, 112.
(27) She, C.; Fedin, I.; Dolzhnikov, D. S.; Dahlberg, P. D.; Engel, G. S.; Schaller, R. D.; Talapin, D. V. Red, Yellow, Green, and Blue Amplified Spontaneous Emission and Lasing Using Colloidal CdSe Nanoplatelets. *ACS Nano* **2015**, *9*, 9475−9485.
(28) Watkins, N. E.; Guan, J.; Diroll, B. T.; Williams, K. R.; Schaller, R. D.; Odom, T. W. Surface Normal Lasing from CdSe Nanoplatelets Coupled to Aluminum Plasmonic Nanoparticle Lattices. *J. Phys. Chem. C* **2021**, *125*, 19874−19879.
(29) Grim, J. Q.; Christodoulou, S.; Di Stasio, F.; Krahne, R.; Cingolani, R.; Manna, L.; Moreels, I. Continuous-wave biexciton lasing at room temperature using solution-processed quantum wells. *Nat. Nanotechnol.* **2014**, *9*, 891−895.
(30) Qiu, L.; Mandal, A.; Morshed, O.; Meidenbauer, M. T.; Girten, W.; Huo, P.; Vamivakas, A. N.; Krauss, T. D. Molecular Polaritons Generated from Strong Coupling between CdSe Nanoplatelets and a Dielectric Optical Cavity. *J. Phys. Chem. Lett.* **2021**, *12*, 5030−5038.
(31) Shlesinger, I.; Monin, H.; Moreau, J.; Hugonin, J. P.; Dufour, M.; Ithurria, S.; Vest, B.; Greffet, J. J. Strong Coupling of Nanoplatelets and Surface Plasmons on a Gold Surface. *ACS Photonics* **2019**, *6*, 2643−2648.
(32) Winkler, J. M.; Rabouw, F. T.; Rossinelli, A. A.; Jayanti, S. V.; McPeak, K. M.; Kim, D. K.; le Feber, B.; Prins, F.; Norris, D. J. Room-Temperature Strong Coupling of CdSe Nanoplatelets and Plasmonic Hole Arrays. *Nano Lett.* **2019**, *19*, 108−115.
(33) Kravets, V. G.; Kabashin, A. V.; Barnes, W. L.; Grigorenko, A. N. Plasmonic Surface Lattice Resonances: A Review of Properties and Applications. *Chem. Rev.* **2018**, *118* (12), 5912−5951.
(34) Zou, S.; Janel, N.; Schatz, G. C. Silver nanoparticle array structures that produce remarkably narrow plasmon lineshapes. *J. Chem. Phys.* **2004**, *120*, 10871−10875.
(35) Cherqui, C.; Bourgeois, M. R.; Wang, D.; Schatz, G. C. Plasmonic Surface Lattice Resonances: Theory and Computation. *Acc. Chem. Res.* **2019**, *52*, 2548−2558.
(36) Wang, W.; Ramezani, M.; Väkeväinen, A. I.; Törmä, P.; Rivas, J. G.; Odom, T. W. The rich photonic world of plasmonic nanoparticle arrays. *Mater. Today* **2018**, *21*, 303−314.
(37) Utyushev, A. D.; Zakomirnyi, V. I.; Rasskazov, I. L. Collective lattice resonances: Plasmonics and beyond. *Rev. Phys.* **2021**, *6*, 100051.
(38) Tan, M. J. H.; Park, J. E.; Freire-Fernández, F.; Guan, J.; Juarez, X. G.; Odom, T. W. Lasing Action from Quasi-Propagating Modes. *Adv. Mater.* **2022**, *34*, 2203999.
(39) Freire-Fernández, F.; Cuerda, J.; Daskalakis, K. S.; Perumbilavil, S.; Martikainen, J. P.; Arjas, K.; Törmä, P.; van Dijken, S. Magnetic on-off switching of a plasmonic laser. *Nat. Photonics* **2022**, *16*, 27−32.
(40) Guo, R.; Nečada, M.; Hakala, T. K.; Väkeväinen, A. I.; Törmä, P. Lasing at K Points of a Honeycomb Plasmonic Lattice. *Phys. Rev. Lett.* **2019**, *122*, 013901.
(41) Hakala, T. K.; Rekola, H. T.; Väkeväinen, A. I.; Martikainen, J.-P.; Nečada, M.; Moilanen, A. J.; Törmä, P. Lasing in dark and bright modes of a finite-sized plasmonic lattice. *Nat. Commun.* **2017**, *8*, 13687.

https://doi.org/10.1021/acsnano.4c03164
ACS Nano 2024, 18, 15177−15184

(42) Moerland, R. J.; Hakala, T. K.; Martikainen, J.-P.; Rekola, H. T.; Väkeväinen, A. I.; Törmä, P. *Strong Coupling Between Organic Molecules and Plasmonic Nanostructures*; Springer, 2017; pp 121−150.
(43) Trinh, Q. T.; Nguyen, S. K.; Nguyen, D. H.; Tran, G. K.; Le, V. H.; Nguyen, H.-S.; Le-Van, Q. Coexistence of surface lattice resonances and bound states in the continuum in a plasmonic lattice. *Opt. Lett.* **2022**, *47*, 1510.
(44) Guan, J.; Sagar, L. K.; Li, R.; Wang, D.; Bappi, G.; Wang, W.; Watkins, N.; Bourgeois, M. R.; Levina, L.; Fan, F.; et al. Quantum Dot-Plasmon Lasing with Controlled Polarization Patterns. *ACS Nano* **2020**, *14*, 3426−3433.
(45) Ithurria, S.; Tessier, M. D.; Mahler, B.; Lobo, R. P. S. M.; Dubertret, B.; Efros, A. L. Colloidal nanoplatelets with two-dimensional electronic structure. *Nat. Mater.* **2011**, *10*, 936−941.
(46) Khan, A. H.; Pinchetti, V.; Tanghe, I.; Dang, Z.; Martín-García, B.; Hens, Z.; Van Thourhout, D.; Geiregat, P.; Brovelli, S.; Moreels, I. Tunable and Efficient Red to Near-Infrared Photoluminescence by Synergistic Exploitation of Core and Surface Silver Doping of CdSe Nanoplatelets. *Chem. Mater.* **2019**, *31*, 1450−1459.
(47) Ji, B.; Rabani, E.; Efros, A. L.; Vaxenburg, R.; Ashkenazi, O.; Azulay, D.; Banin, U.; Millo, O. Dielectric Confinement and Excitonic Effects in Two-Dimensional Nanoplatelets. *ACS Nano* **2020**, *14*, 8257−8265.
(48) Tessier, M. D.; Javaux, C.; Maksimovic, I.; Loriette, V.; Dubertret, B. Spectroscopy of single CdSe nanoplatelets. *ACS Nano* **2012**, *6*, 6751−6758.
(49) Rowland, C. E.; Fedin, I.; Zhang, H.; Gray, S. K.; Govorov, A. O.; Talapin, D. V.; Schaller, R. D. Picosecond energy transfer and multiexciton transfer outpaces Auger recombination in binary CdSe nanoplatelet solids. *Nat. Mater.* **2015**, *14*, 484−489.
(50) Auguié, B.; Barnes, W. L. Collective resonances in gold nanoparticle arrays. *Phys. Rev. Lett.* **2008**, *101*, 143902−143904.
(51) Barnes, W. L.; Preist, T. W.; Kitson, S. C.; Sambles, J. R. Physical origin of photonic energy gaps in the propagation of surface plasmons on gratings. *Phys. Rev. B: Condens. Matter Mater. Phys.* **1996**, *54*, 6227−6244.
(52) Lu, L.; Le-Van, Q.; Ferrier, L.; Drouard, E.; Seassal, C.; Nguyen, H. S. Engineering a light-matter strong coupling regime in perovskite-based plasmonic metasurface: quasi-bound state in the continuum and exceptional points. *Photon. Res.* **2020**, *8*, A91.
(53) Hoang, T. B.; Akselrod, G. M.; Yang, A.; Odom, T. W.; Mikkelsen, M. H. Millimeter-Scale Spatial Coherence from a Plasmon Laser. *Nano Lett.* **2017**, *17*, 6690−6695.
(54) Zhang, Q.; Zhu, Y.; Niu, P.; Lao, C.; Yao, Y.; Liu, W.; Yang, Q. F.; Chu, S.; Gao, Y. Low-Threshold Single-Mode Microlasers from Green CdSe/CdSeS Core/Alloyed-Crown Nanoplatelets. *ACS Photonics* **2023**, *10*, 1397−1404.
(55) Yang, H.; Zhang, L.; Xiang, W.; Lu, C.; Cui, Y.; Zhang, J. Ultralow Threshold Room Temperature Polariton Condensation in Colloidal CdSe/CdS Core/Shell Nanoplatelets. *Adv. Sci.* **2022**, *9*, 2200395.
(56) Huang, C.; Zhang, C.; Xiao, S.; Wang, Y.; Fan, Y.; Liu, Y.; Zhang, N.; Qu, G.; Ji, H.; Han, J.; et al. Ultrafast control of vortex microlasers. *Science* **2020**, *367*, 1018−1021.
(57) Deng, H.; Weihs, G.; Snoke, D.; Bloch, J.; Yamamoto, Y. Polariton lasing vs. photon lasing in a semiconductor microcavity. *Proc. Natl. Acad. Sci. U.S.A.* **2003**, *100*, 15318−15323.
(58) Berghuis, A. M.; Tichauer, R. H.; de Jong, L. M. A.; Sokolovskii, I.; Bai, P.; Ramezani, M.; Murai, S.; Groenhof, G.; Gomez Rivas, J. Controlling Exciton Propagation in Organic Crystals through Strong Coupling to Plasmonic Nanoparticle Arrays. *ACS Photonics* **2022**, *9* (7), 2263−2272. From NLM PubMed-not-MEDLINE
(59) Koessler, E. R.; Mandal, A.; Huo, P. Incorporating Lindblad decay dynamics into mixed quantum-classical simulations. *J. Chem. Phys.* **2022**, *157*, 064101.

https://doi.org/10.1021/acsnano.4c03164
ACS Nano 2024, 18, 15177−15184